# NOTICE CONCERNING COPYRIGHT RESTRICTIONS

# Relationship between Rate of Aperture Reduction and Contact Pressure of Fracture in Granite under Hydrothermal Condition

**Noriaki Watanabe, Hiroshi Iijima, Nobuo Hirano, and Noriyoshi Tsuchiya**

**Graduate School of Environmental Studies, Tohoku University, Sendai, Japan**

***Keywords***

*Aperture reduction, contact pressure, granite fracture, hydrothermal condition, EGS*

## ABSTRACT

A coupled experimental and numerical analysis was performed on artificial fractures of granite in order to evaluate a relationship between a rate of aperture reduction and a contact pressure under hydrothermal conditions. In the experimental work, distilled water was injected into the fractures of 150 °C at the different effective confining pressures of 16 and 25 MPa during several tens of hours. At both the effective confining pressures, the fracture permeabilities decreased non-monotonically with time. Since Si concentrations of effluents were far from saturation over the range of experiments, the predominant reaction within the fractures was dissolution of rock-forming minerals. In addition, the surface mapping did not show significant changes in the fracture surface roughness between before and after the experiment, suggesting that the permeability reductions originated mainly from the aperture reductions by pressure solution of contacting asperities. The rates of aperture reduction were therefore evaluated on the basis of the numerical modeling of the aperture structures during the experiment. The numerically determined changes in the aperture reduction and the contact pressure of the fractures provided the rates of aperture reduction of 1.0-6.4 μm/hour for the contact pressures of 35-54 MPa. Although the relationship between the aperture reduction and the contact pressure was far from one-to-one, the rate of aperture reduction seemed to grow exponentially with an increase of contact pressure.

## Introduction

For effective development of geothermal, particularly the Enhanced Geothermal System (EGS), reservoirs, it is necessary to understand hydrothermal flow within rock fractures. In our recent coupled experimental-numerical studies for water flow through artificially created fractures of granite, channeling flow (developments of preferential flow paths) has been observed in heterogeneous aperture structures of the fractures (Watanabe *et al*., 2008). Although various types of aperture structures were observed depending on geological conditions, channeling flow occurred in every aperture structure at a wide range of effective confining pressures of 10-100 MPa. It is therefore suggested that channeling flow usually occurs in rock fractures in geothermal reservoirs. Since the heterogeneous aperture/flow structures are thought to change with time by modifications of fracture surface geometries (e.g. mineral dissolution and/or precipitation) under hydrothermal conditions, it is significant to understand and model the changes of the heterogeneous structures in order to optimize permeability and heat exchange effectiveness of rock fractures.

We previously performed a coupled experimental-numerical analysis on changes of aperture/flow structures within an artificial fracture in granite during Si-supersaturated water injection (Watanabe *et al*., 2007). As a result, the flow structure was drastically changed with time due to mineral precipitation on preferential flow paths developed in the aperture structure. In addition, no significant change in number of contacting asperities (contact area) was observed, suggesting the changes of aperture/flow structures at such condition can be predicted by the numerical simulation on the basis of geochemical reactions and material transports as found in a previous study (O'Brien *et al*., 2003). On the other hand, at the conditions of far-from-saturation water injection, which may be more likely in developments of geothermal reservoirs, it is suggested to incorporate pressure solution at contacting asperities into the numerical simulation (Yasuhara and Elsworth, 2004). The rate of pressure solution, i.e. rate of aperture reduction, may be described as a function of average pressure of contacting asperities within a rock fracture (contact pressure, $P_c$) that is calculated by the contact area, $A_c$, and the effective confining pressure, $\sigma_e$:

$$P_c = \sigma_e \frac{100}{A_c} \quad , \tag{1}$$

where the contact area is the percentage of area of contacting asperities within a rock fracture.

However, the relationship between the rate of aperture reduction and the contact pressure has not been clear due to difficulties in experimental measurements of the contact area and/or the rate of aperture reduction under hydrothermal conditions.

The objective of the present study is therefore to evaluate the relationship between the rate of aperture reduction and the contact pressure, on the basis of the coupled experimental-numerical analysis of aperture/flow structures that we previously developed. First, a hydrothermal flow-through experiment was performed on artificial fractures of granite under conditions of Si-far-from-saturation water injection, in order to detect aperture reductions by the pressure solution as permeability reductions. In the experiment, Si concentrations of effluents and fracture surface roughness were also evaluated in order to confirm that the aperture reductions originated mainly from pressure solution at contacting asperities. Aperture changes and contact areas were then evaluated by numerical modeling of aperture structures on the basis of the experimental results, providing the relationship between the rate of aperture reduction and the contact pressures.

## Methods

### *Hydrothermal Flow-Through Experiment*

Two cylindrical granite samples that contained single artificial fractures were prepared from Iidate medium-grained granite (Fukushima, Japan). The samples were 50 mm in diameter and 120 mm in length. Since the fractures were contained along the long axis of the samples, the dimensions of the fractures were 50 mm x 120 mm. For the evaluation of surface roughness and the numerical modeling of the aperture structures, surface mapping was performed on the fractures before and after the experiment by using a laser-scanning equipment (accuracy of positioning: +/- 20 μm, resolution of asperity heights: 10 μm). The fracture surfaces were measured in 250-μm square grid system, providing 200 x 480 data points for each surface. In the evaluation of surface roughness, the roughness coefficient ($Z_2$) and the tortuosity ($\tau$) were calculated:

$$Z_2 = \sqrt{\frac{1}{N-1}\sum_{i=0}^{N-2}\left(\frac{z_{i+1}-z_i}{\Delta x}\right)^2}\ , \tag{2}$$

$$\tau = \frac{\sum_{i=0}^{N-2}\sqrt{\left(z_{i+1}-z_i\right)^2+\left(\Delta x\right)^2}}{L}\ , \tag{3}$$

where $z_i$ is the asperity height, $\Delta x$ is the distance between adjacent data points, $L$ is the apparent length, and $N$ is the number of the data points, with respect to a 2-D ($x$- or $y$-$z$) surface profile [*Sausse*, 2002]. The roughness coefficient is defined as the root mean square of local slopes, providing the measure of the microscopic (grid-scale) roughness. On the other hand, the tortuosity is defined as the ratio of the real length to the apparent length of the profile, providing macroscopic (sample-scale) roughness.

The experimental system of the hydrothermal flow-through experiment is shown in Figure 1. The system was developped using the Rubber-Confining Pressure Vessel (Hirano *et al*., 2005; Watanabe *et al*., 2006). The Rubber-Confininig Pressure Vessel (R-CPV) with the sample was placed in the pressing machine. By controlling the load of the pressing machine, prescribed confining pressure was applied to the sample. Distilled water was injected into the fracture at a prescribed flow rate using the pump. In the R-CPV, a prescribed effective confining pressure was applied to the sample by controlling the pore pressure using the pressure regulating valve. Prescribed temperature was maintained using the heating jacket surrounding the R-CPV. In the present study, effective pressure of either 16 MPa or 25 MPa was applied to each sample, although the temparature and the flow rate were always 150 °C and 10 ml/min, respectively.

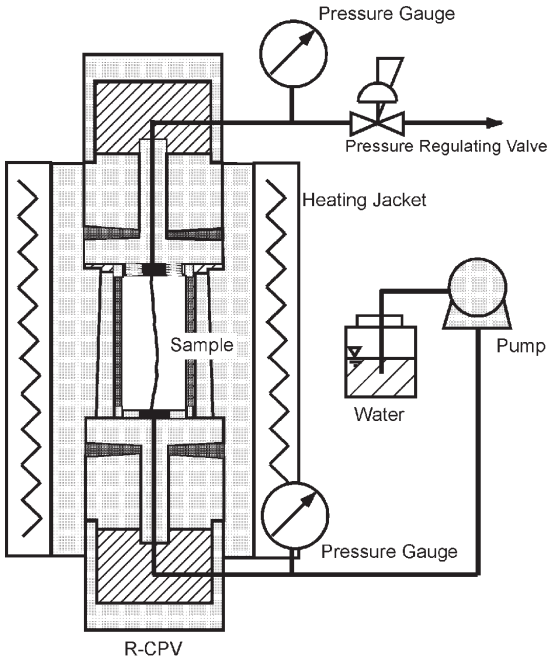


**Figure 1.** Experimental system of the hydrothermal flow-through experiment for the artificial fractures of granite.

In the experiment, the hydraulic pressure differeces between the inlet and the outlet sides of the fractures was measured at every prescribed time to evaluate permeability changes during the experiment. Fracture permeability was calculated on the basis of the cubic law assumption using the dimensions of fracture, the water viscosity, the hydraulic pressure differece and the flow rate (see, Equations (5) and (6) in the next subsection). In addition, Si concentrations of effluents were evaluated with ICP-AES to infer predominant reaction within the fracture.

### *Numerical Modeling*

The numerical model, which incorporates the experimentally obtained surface geometries and permeabilities, was used for the determination of the aperture structures of the fractures (Watanabe *et al*., 2008). The aperture structures will provide changes in aperture reduction and contact pressure with time in the next section. The outline of the numerical modeling can be described as below. A model of an aperture structure is constructed on a computer by using the experimentally obtained digital data of fracture surface geometries. The local cubic law (LCL) based flow-through simulation is performed for the model under the same boundary conditions as those described in the experiment. Based on the simulation, permeability of the model is evaluated using

the same equations as those described in the experiment as well, and the permeability is compared with the experimentally obtained fracture permeabilities. By matching the numerical permeability with the experimental one through a modification of the model (normal displacement), the numerical aperture structure having the experimental permeability can be determined.

In the present study, the model of the aperture structure was represented by the 2-D distribution of local apertures, where the local apertures were represented by vertical separations between opposite fracture surfaces. The model with at least a single contacting asperity was initially constructed, and the model was then modified through the simulation for the normal displacement (closer) to match the permeability of a model with the experimentally obtained fracture permeability. In the modification, all local apertures were reduced uniformly and overlapped asperities simply created zero local apertures, i.e. contacting asperities (Power and Durham, 1997; van Genabeek and Rothman, 1999; Matsuki *et al*., 2006). It is noted that the zero local apertures were subsutituted by significant small local apertures of 0.1 μm for the flow-through simulation described below.

The 3-D flow of incompressible and viscous fluid (water) through the aperture structure was approximated by the Reynolds equation (Mourzenko *et al*., 1995; Yeo *et al*., 1998; Ge, 1997; Oron and Berkowitz, 1998; Pyrak-Nolte and Morris, 2000; Brush and Thomson, 2003; Konzuk and Kueper, 2004):

$$\frac{\partial}{\partial x}\left(\frac{e^3}{12\mu}\frac{\partial P}{\partial x}\right)+\frac{\partial}{\partial y}\left(\frac{e^3}{12\mu}\frac{\partial P}{\partial y}\right)=0 \ , \tag{4}$$

where $e$ is the local aperture, $\mu$ is the water viscosity and $p$ is the hydraulic pressure.

Linear equations derived from a finite difference form of Equation (4) were solved using a simulator, the D/SC (Tezuka and Watanabe, 2000), by substituting contacting asperities with 0.1 μm local apertures, and by assuming constant water viscosity, for convenience. Boundary conditions were given such that macroscopic water flow occurred in one direction. The condition of constant pressure (constant macroscopic pressure gradient) was given for boundaries perpendicular to the direction of macroscopic flow, and the condition of non-flow was given for boundaries parallel to the direction of macroscopic flow.

The hydraulic aperture ($e_h$) was calculated using the following equation (Brown, 1987; Chen *et al*., 2000):

$$e_h=\left(\frac{12\mu Q}{W(\Delta P/L)}\right)^{1/3} \tag{5}$$

where $Q$ is the flow rate, $W$ and $L$ are the length of the boundaries perpendicular and parallel to the macroscopic flow and $\Delta P/L$ is the macroscopic pressure gradient. In addition, permeability ($k$) was calculated using the following equation:

$$k=\frac{e_h^2}{12} \tag{6}$$

## Results and Discussion

Figure 2 shows the experimentally observed permeability changes of the granite fractures with time at the effective confining pressures of 16 MPa and 25 MPa. At both the effective confining pressures, the temperature and the flow rate were 150 °C and 10 ml/min, respectively. The difference in the effective confining pressure caused the difference in the initial permeabilities at 0 hour. However, the permeability changes were similar in the both cases, showing the non-monotonic permeability reductions with time. The rates of the reduction were significantly decreased approximately at 22.2 hours and 14.8 hours for 16 MPa and 25 MPa, respectively.

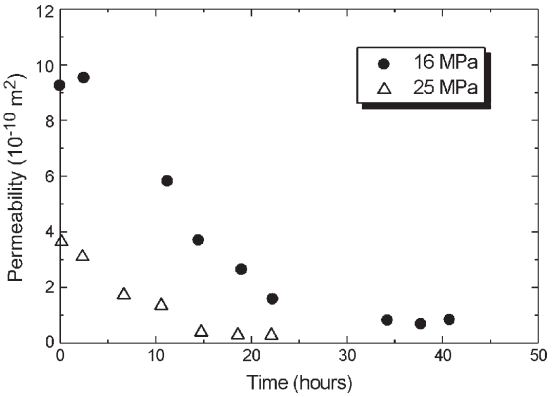


**Figure 2.** Experimentally observed permeability changes of the granite fractures with time at the effective confining pressures of 16 MPa and 25 MPa. At both the effective confining pressures, the temperature and the flow rate are 150 °C and 10 ml/min, respectively.

The observed Si concentrations of effluents were less than 10 ppm over the experiment. This much smaller concentrations compared with the solubility at 150 °C indicated that the predominant reaction within the fractures was dissolution of rock-forming minerals. In addition, the differences in the roughness coefficient and the tortuosity between before and after the experiment were usually less than several percent (-1.7% in the roughness coefficient, and -0.37 % in the tortuosity), suggesting the changes in the aperture structures occurred in limited regions within the fractures. It can therefore be assumed that the observed permeability reductions were originated mainly from pressure solution at contacting asperities.

Figure 3, overleaf, shows the numerically determined aperture/flow structures of the granite fracture at the initial and the final states for the experiments at the effective confining pressure of 16 MPa. The changes in the aperture structure by the experiment were remarkable particularly in the increase of contact area, resulting in the drastic flow path changes. Since the increase of contact area represented a decrease of contact pressure, the numerical observation was in harmony with the decreases in the rate of permeability reduction, i.e. the rate of aperture reduction by pressure solution.

For evaluation of the relationship between the rate of aperture reduction and the contact pressure, it was necessary to determine aperture structures not only at the initial and the final states but also during the experiments. This required the data of fracture surface geometries during the experiments, which was however usually impossible to obtain. The aperture structures during the experiments were therefore determined by using the data that was obtained before the experiment, on the assumption that no significant changes in fracture surface geometries occurred during

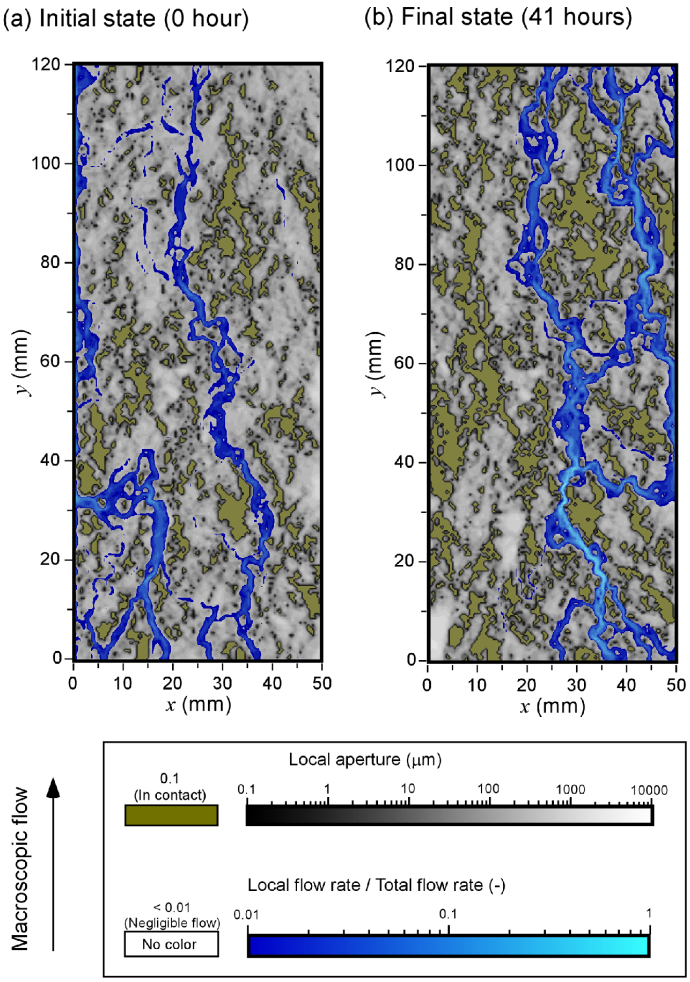


**Figure 3.** Numerically determined aperture/flow structures of the granite fracture at the initial and the final states for the experiments at the effective confining pressure of 16 MPa.

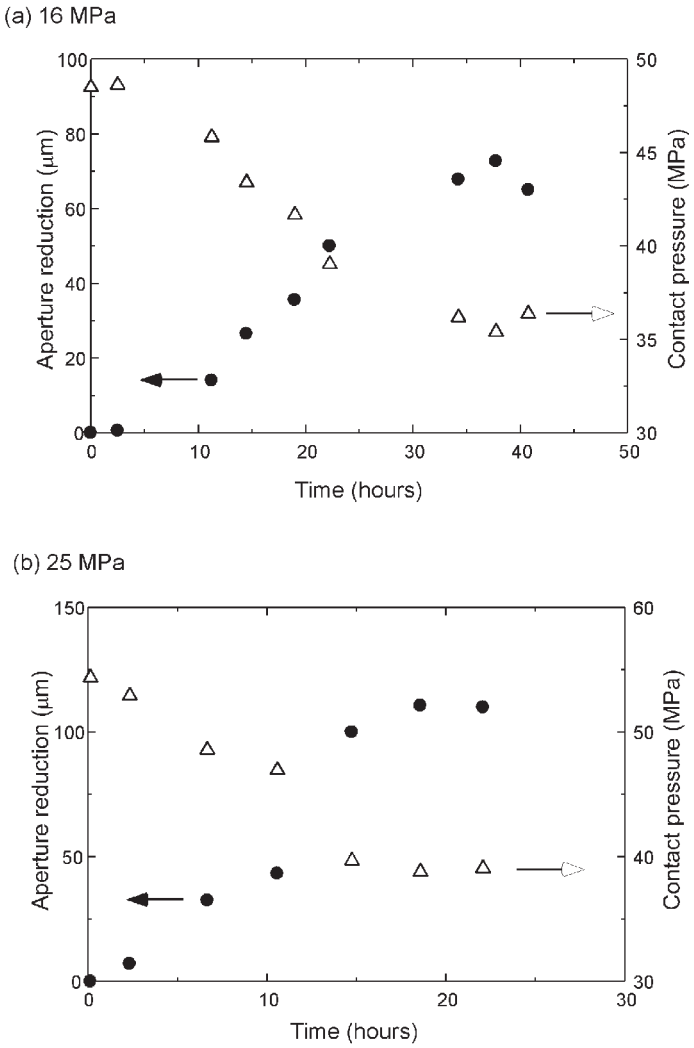


**Figure 4.** Numerically determined changes in the aperture reduction and the contact pressure of the granite fractures with time for the experiment at the effective confining pressures of 16 MPa (a) and 25 MPa (b).

the relatively short-duration experiment in the present study. This assumption was thought to be reasonable since no significant change was really found both in the roughness coefficient and in the tortuosity.

Figure 4 shows the numerically determined changes in the aperture reduction and the contact pressure of the granite fracture with time for the experiment at the effective confining pressures of 16 MPa and 25 MPa. The aperture reduction became greater with time, in response to the experimental permeability reductions. Since the aperture reduction caused an increase of the contact area, the contact pressure became smaller with time. In the experiment, the rate of permeability reduction changed at 22.2 hours and 14.8 hours for 16 MPa and 25 MPa, respectively. Consequently, the rates of aperture reduction changed at these points, dividing the experiment into two domains where the relationships between the aperture reduction and the time were roughly linear. The rates of aperture reduction were therefore determined as the slopes of linear curves derived from the least squares method as shown in Figure 5, resulting in the rates of 1.0-6.4 μm/hour. On the other hand, since the contact pressures changed even when the rates were apparently constant, it was suggested that the rate of aperture reduction and the contact pressure did not have one-to-one relationship.

Figure 6 shows the relationship between the rate of aperture reduction and the contact pressure of the granite fracture at 150 °C. The white symbols represent the maximum and minimum contact pressures, and the black symbols represent the average contact pressures. Although the relationship was far from one-to-one, a rate of aperture reduction seemed to grow exponentially with an increase of contact pressure at constant temperature, providing fundamental insights into the relationship between the aperture reduction by pressure solution and the contact pressure at contacting asperities.

## Conclusions

We performed the coupled experimental-numerical analysis on the artificial fractures of granite at 150 °C in order to evaluate the relationship between the rate of aperture reduction by pressure solution and the contact pressure at contacting asperities within the fracture. The experimental results showed permeability reductions with time under the condition of far-from-saturation water

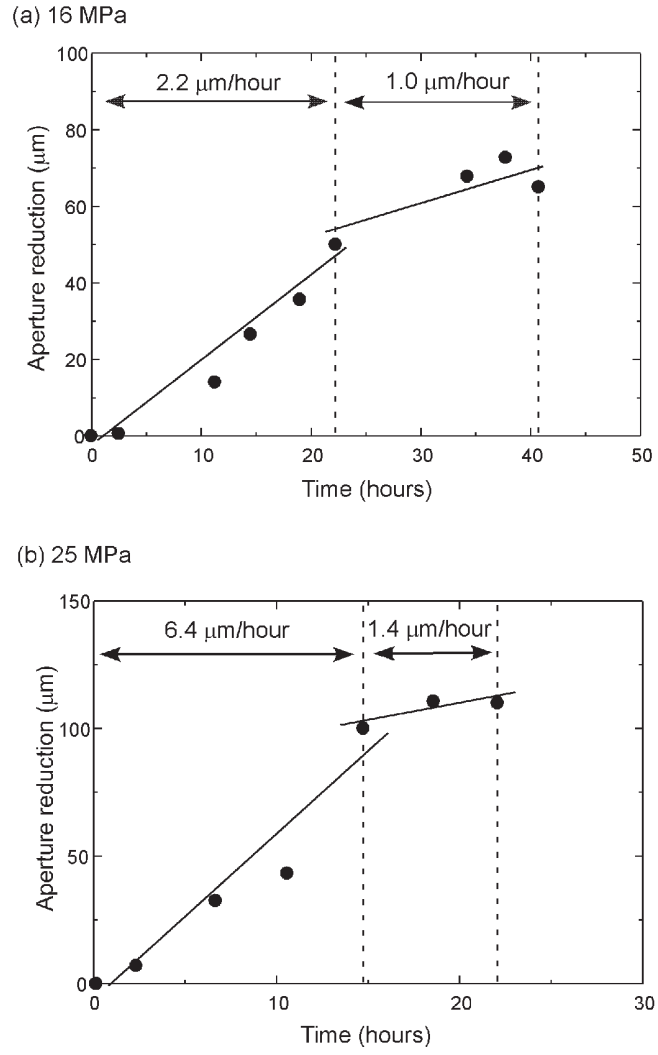


**Figure 5.** Determination of the rates of aperture reduction of the granite fractures at the effective confining pressures of 16 MPa (a) and 25 MPa (b), on the basis of the numerical results shown in Figure 4.

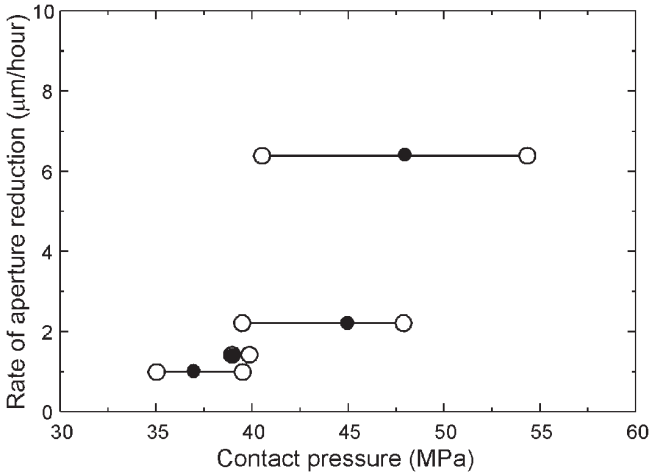


**Figure 6.** Relationship between the rate of aperture reduction and the contact pressure of the granite fracture. The white symbols represent the maximum and minimum contact pressures, and the black symbols represent the average contact pressures for each rate of aperture reduction.

injection. According to the significant small Si concentrations of effluents and the fracture surface roughness changes, the permeability reductions was thought to result manly from the aperture reductions by pressure solution. The numerical results provided the rates of aperture reductions of 1.0-6.4 μm/hour for 35-54 MPa. Although a one-to-one relationship was not found between the rate of aperture reduction and the contact pressure, a rate of aperture reduction seemed to grow exponentially with an increase of contact pressure at constant temperature.

## Acknowledgements

The authors would like to thank Dr. Kimio Watanabe (Rich Stone Limited) for assistance in the flow-through simulations with the D/SC.

## References

Brown, S. R. (1987), Fluid flow through rock joints: The effect of surface roughness, *J. Geophys. Res.*, *92* (B2), 1337-1347.

Brush, D. J. and N. R. Thomson (2003), Fluid flow in synthetic rough-walled fractures: Navier-Stokes, Stokes, and local cubic law assumptions, *Water Resour. Res.*, *39* (4), 1085, doi:10.1029/2002WR001346.

Chen, Z., S. P. Narayan, Z. Yang and S. S. Rahman (2000), An experimental investigation of hydraulic behavior of fractures and joints in granitic rock, *Int. J. Rock Mech. Min. Sci.*, *37* (7), 1061-1071.

Ge, S. (1997), A governing equation for fluid flow in rock fractures, *Water Resour. Res.*, *33* (1), 53-61.

Hirano, N., N. Watanabe and N. Tsuchiya, (2005), Development of rubber confining pressure vessel and flow test using this apparatus, *J. Min. Mater. Process. Inst. JPN.*, *121*, 484-488 (in Japanese with English abstract).

Konzuk, J. S. and B. H. Kueper (2004), Evaluation of cubic law based models describing single-phase flow through a rough-walled fracture, *Water Resour. Res.*, *40*, W02402, doi:10.1029/2003WR002356.

Matsuki, K., Y. Chida, K. Sakaguchi and P. W. J. Glover (2006), Size effect on aperture and permeability of a fracture as estimated in large synthetic fractures, *Int. J. Rock Mech. Min. Sci.*, *43* (5), 726-755.

Mourzenko, V. V., J. -F. Thovert and P. M. Adler (1995), Permeability of a single fracture: validity of the Reynolds equation, *J. Phys II France*, *5* (3), 465-482.

Oron, A. P. and B. Berkowitz (1998), Flow in rock fractures: the local cubic law assumption reexamined, *Water Resour. Res.*, *34* (11), 2811-2825.

O'Brien, G. S., C. J. Bean and F. McDermott (2003), Numerical investigations of passive and reactive flow through generic single fractures with heterogeneous permeability, *Earth Planet. Sci. Lett.*, *213*, 271-284.

Power, W. L. and W. B. Durham (1997), Topography of natural and artificial fractures in granitic rocks: Implication for studies of rock friction and fluid migration, *Int. J. Rock Mech. Min. Sci.*, *34* (6), 979-989.

Pyrak-Nolte, L. J. and J. P. Morris (2000), Single fractures under normal stress: The relation between fracture specific stiffness and fluid flow, *Int. J. Rock Mech. Min. Sci.*, *37* (1-2), 245-262.

Sausse, J. (2002), Hydromechanical properties and alteration of natural fracture surfaces in the Soultz granite (Bas-Rhin, France), *Tectonophysics*, *348* (1), p. 169-185.

Tezuka, K. and K. Watanabe (2000), Fracture network modeling of Hijiori hot dry rock reservoir by deterministic and stochastic crack network simulator (D/SC), *Proc. World Geotherm. Cong. 2000*, 3933-3938.

van Genabeek, O. and D. H. Rothman (1999), Critical behavior in flow through a rough-walled channel, *Phys. Lett. A*, *255* (1-2), 31-36.

Watanabe, N., N. Hirano, T. Tamagawa, K. Tezuka and N. Tsuchiya (2006), Fundamental study for prediction of productivity in oil/gas fractured reservoir based on flow-through experiment under confining pressure, *J. Jpn. Assoc. Petrol. Tech.*, *71* (2), 217-226 (in Japanese with English abstract).

Watanabe, N., N. Hirano and N. Tsuchiya (2008), Determination of aperture structure and fluid flow in a rock fracture by high-resolution numerical modeling on the basis of a flow-through experiment under confining pressure, *Water Resour. Res., in press*.

Watanabe, N., H. Iijima, N. Hirano and N. Tsuchiya (2007), Observation of flow path change in rock fracture under hydrothermal condition using a coupled experimental-numerical method, *Geotherm. Resour. Council Trans.*, *31*, 323-327.

Yasuhara, H. and D.Elsworth (2004), Evolution of permeability in a natural fracture: Significant role of pressure solution, *J. Geophys. Res.*, *109*, B03204, doi:10.1029/2003JB002663.

Yeo, I. W., M. H. de Freitas and R. W. Zimmerman (1998), Effect of shear displacement on the aperture and permeability of a rock fracture, *Int. J. Rock Mech. Min. Sci.*, *35* (8), 1051-1070.